^{51}V NMR evidence for interlayer-modulated charge order and a first-order low-temperature transition in CsV_3Sb_5

Xiaoling Wang [1,*] Arneil P. Reyes [2] Hrishit Banerjee [3] Andrea N. Capa Salinas [4] Stephen Wilson,[4] and Brenden R. Ortiz [5]

[1]*Department of Chemistry and Biochemistry, California State University East Bay, Hayward, California 94542, USA*
[2]*National High Magnetic Field Laboratory, Tallahassee, Florida 32310, USA*
[3]*University of Dundee, Dundee DD1 4HN, Scotland, United Kingdom*
[4]*Materials Department, University of California, Santa Barbara, California 93106, USA*
[5]*Materials Science and Technology Division, Oak Ridge National Laboratory, Oak Ridge, Tennessee 37831, USA*

(Received 4 September 2025; revised 31 October 2025; accepted 12 November 2025; published 8 December 2025)

Charge order in the kagome superconductor CsV_3Sb_5 exhibits a complex three-dimensional organization and intermediate-temperature anomalies whose bulk character has remained unsettled. We use orientation-dependent ^{51}V NMR as a site-selective probe to determine the stacking of the charge density wave (CDW) state and its thermal evolution. Below $T_{CDW} \approx 94$ K, the field-linear splitting of the ^{51}V central transition together with the anisotropy of the Knight shift tensor identify an interlayer-modulated $3q$ CDW whose local environments are consistent with a four-layer $2 \times 2 \times 4$ stacking with mixed trihexagonal/Star-of-David distortions, in agreement with synchrotron x-ray determinations. For comparison, RbV_3Sb_5 serves as a reference exhibiting a uniform trihexagonal $2 \times 2 \times 2$ stacking, allowing us to isolate features unique to the $2 \times 2 \times 4$ state in CsV_3Sb_5. With $H_0 \parallel c$, the ^{51}V quadrupolar satellites through the intermediate temperature scale near $T_{CO} \approx 65$ K reorganize into two well-resolved electric-field-gradient manifolds that coexist over a finite interval; their relative spectral weights interchange on cooling while the total integrated satellite intensity remains conserved and ν_Q within each manifold is nearly temperature independent. The coexistence without critical broadening, together with conserved intensity, provides bulk evidence consistent with a first-order charge-order transition near T_{CO}. Our measurements do not resolve whether this lower-temperature transition corresponds to a distinct in-plane order or a reorganization of the $3q$ state; rather, they delimit this window and provide bulk, site-resolved constraints that connect prior reported anomalies to a thermodynamic first-order transition.

DOI: 10.1103/91c9-z267

I. INTRODUCTION

The recent discovery of the kagome superconductors AV_3Sb_5 (A = K, Rb, Cs) has stimulated extensive research, particularly focusing on their complex charge density wave (CDW) states [1–3]. In these materials, CDW formation is closely tied to Fermi surface nesting and proximity to van Hove singularities (VHSs) near the Fermi level [4–8]. The CDW phase involves subtle structural distortions within the vanadium sublattice, establishing a three-dimensional ordered state with well-defined phase coherence across the kagome planes [9,10]. The distortion is characterized by a $3q$ breathing mode pattern, forming a trihexagonal (TrH) or a Star-of-David (SoD) arrangement. Whereas KV_3Sb_5 and RbV_3Sb_5 predominantly exhibit a staggered TrH pattern, CsV_3Sb_5 displays a more intricate arrangement [11,12]. Scanning tunneling microscopy (STM) studies have reported alternating layers of SoD and TrH distortions, highlighting the intricate layered nature of the CDW order [13]. Synchrotron x-ray diffraction reveals that the CDW evolves from intermediate $2 \times 2 \times 1$ and $2 \times 2 \times 2$ superstructures to a stable $2 \times 2 \times 4$ phase at lower temperatures, characterized by specific stacking patterns of SoD and TrH distortions [14]. Raman spectroscopy experiments have identified pronounced phonon anomalies indicative of strong electron-phonon coupling involved in CDW formation [15]. Complementary density functional theory (DFT) and angle-resolved photoemission spectroscopy (ARPES) attribute the CDW instabilities primarily to electronic nesting involving vanadium-derived VHS near the M and L points of the Brillouin zone [4,5]. Furthermore, coherent phonon spectroscopy provides direct evidence of simultaneous phonon condensation at these critical wave vectors, underscoring the multimodal character of the CDW transition [16].

In this study, we use angle-resolved ^{51}V NMR as a bulk, site-selective probe to address two open issues. First, while synchrotron x-ray and STM have established that CsV_3Sb_5 often hosts a mixed-layer CDW with a $2 \times 2 \times 4$ modulation distinct from the uniform staggered-TrH $2 \times 2 \times 2$ order in RbV_3Sb_5, a direct, bulk spectroscopic discriminator between these three-dimensional microstructures has been lacking. Second, although surface- and optical-probe measurements

*Contact author: xiaoling.wang@csueastbay.edu

including polarizationresolved Raman spectroscopy studies of CDW induced phonon anomalies and spectroscopic imaging scanning tunneling microscopy (SI-STM) reports of $4a_0$ "stripe like" modulation have revealed anomalies near 60 K in CsV_3Sb_5, they do not establish a bulk symmetry-lowering phase transition or determine its thermodynamic order. For comparison, RbV_3Sb_5 serves as a reference exhibiting a uniform stacking pattern, allowing us to isolate features unique to CsV_3Sb_5. We show that the ^{51}V Knight shift tensor cleanly separates the interlayer-modulated CDW microstructures of CsV_3Sb_5 and RbV_3Sb_5 right below T_{CDW}, providing a bulk spectroscopic discriminator consistent with the diffraction-inferred stacking in each compound. To our knowledge, prior NMR/nuclear quadrupole resonance (NQR) studies did not explicitly delineate this Rb-Cs contrast via a Knight shift splitting immediately below T_{CDW} [17–26]; earlier evidence for differing stacking largely came from diffraction and STM. Here we establish a bulk, site-resolved discriminator between the $2 \times 2 \times 4$ (Cs) and $2 \times 2 \times 2$ (Rb) CDW stackings, complementing prior diffraction/STM identifications. At lower temperatures in CsV_3Sb_5 the ^{51}V quadrupolar satellites reorganize into two coexisting electric field gradient (EFG) environments, establishing bulk evidence consistent with a first-order charge-order transition into a symmetry-lowered phase. DFT calculations reproduce the increased spread of EFG anisotropy and point to enhanced in-plane V-d/Sb-p hybridization. While NMR does not determine the in-plane wave vector, these fingerprints are compatible with the unidirectional ($4a_0$) correlations seen by SI-STM near this temperature scale, and therefore reveal a bulk first-order transformation near $T_{CO} \approx 65$ K.

II. EXPERIMENTAL METHODS

A. NMR Methods

Orientation-dependent ^{51}V NMR experiments were performed on single-crystal samples of CsV_3Sb_5 and RbV_3Sb_5, prepared with optimized crystalline quality for accurate spectral measurements, following the procedure in previous reports [1,2]. All NMR measurements used a specialized two-axis rotation device (illustrated in Supplemental Material Fig. S1 [27]), essential for resolving subtle electronic and lattice modulations associated with CDW transitions.

Angle-resolved spectra were acquired by rotating the crystal with respect to the static field H_0 using a two-axis goniometer. We define ϕ as the azimuthal rotation about the crystallographic c axis within the ab plane and θ as the polar angle between H_0 and the c axis ($\theta = 0^\circ$ for $H_0 \| c$, $\theta = 90^\circ$ for $H_0 \| ab$; see Fig. S2 and Supplemental Material Sec. I A). This rigorous orientation control allowed for the distinct identification and characterization of unique vanadium sites emerging at and below the CDW transition temperatures. The detailed analysis involved the extraction of the Knight shift (K) and EFG (V) tensor components from the angle-dependent spectral patterns. These tensors were determined by exact diagonalization of the Zeeman and quadrupole Hamiltonians for the ^{51}V nuclei, followed by precise mathematical transformations among the crystal lattice, the rotation

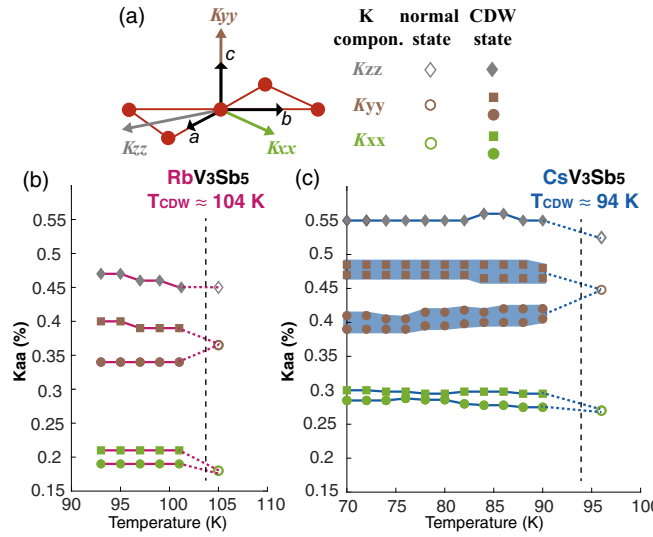

FIG. 1. ^{51}V Knight shift tensor through the CDW transition in RbV_3Sb_5 and CsV_3Sb_5. (a) Definition of principal components with respect to crystal axes. Temperature dependence of K_{xx}, K_{yy}, and K_{zz} in RbV_3Sb_5 across $T_{CDW} \approx 104$ K (b) and for CsV_3Sb_5 across $T_{CDW} \approx 94$ K (c). Circles and squares denote the higher- and lower-frequency central-transition components.

device axes, and the tensor coordinates, as illustrated in Supplemental Material Sec. I A.

B. DFT Calculations

Structural relaxations within DFT were performed using a plane-wave basis set and projector-augmented wave potentials [28], as implemented in the Vienna *Ab initio* Simulation Package (VASP) [29,30].

In all our DFT relaxation calculations, we used the generalized gradient approximation using the Perdew-Burke-Ernzerhof exchange-correlation functional [31]. Ionic relaxations were performed using VASP, allowing internal atomic positions to relax until the forces were less than 0.005 eV/Å. An energy cutoff of 600 eV and an $8 \times 8 \times 4$ Monkhorst-Pack k-point mesh ensured good convergence of the total energy. Computational details regarding the EFG tensor are included in Supplemental Material Sec. II A.

III. RESULTS AND DISCUSSION

A. Knight shift splitting and implications for the CDW superstructures

We performed exact diagonalization of the combined Zeeman and quadrupole Hamiltonians for each distinct vanadium site, fitting angle-dependent ^{51}V NMR spectral data measured at multiple crystal orientations. Through systematic fitting of these angular dependencies, we determined tensor components for each nonequivalent vanadium site, capturing local spin-density modulations induced by the CDW. The anisotropy of the Knight shift provides a sensitive probe of both the in-plane 2×2 reconstruction and the interlayer phasing of the charge order.

Specifically, below T_{CDW}, as illustrated in Fig. 1, our analysis clearly revealed that the Knight shift component in the

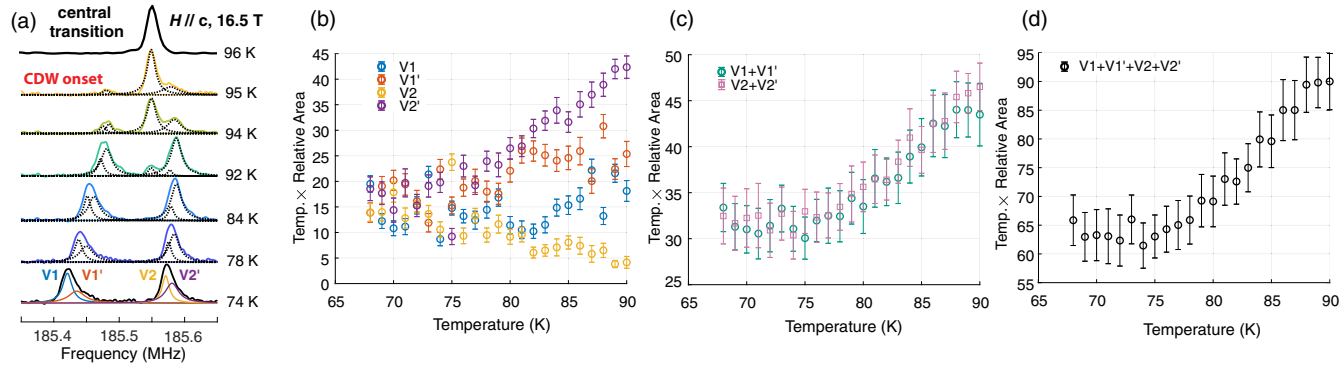

FIG. 2. Temperature evolution of the ^{51}V central transition and component intensities in CsV_3Sb_5 ($H_0 \parallel c$). (a) Stacked central-transition spectra measured at 16.5 T for selected temperatures. The weak two-component structure that appears at 95 K reflects incipient CDW domains. (b) Boltzmann-corrected integrated areas $I(T)T$ for the four fitted components (V1,V1′,V2,V2′). (c) Pairwise sums $I(T)T$ for V1+V1′ and V2+V2′. (d) Total $I(T)T$. Error bars are fit uncertainties.

plane (K_{xx}), oriented in the kagome plane, splits into two distinct resonances below the CDW transition, reflecting the formation of two crystallographically distinct vanadium sites in both RbV_3Sb_5 and CsV_3Sb_5. The perpendicular in-plane component (K_{zz}) remains unsplit in both the Cs and the Rb variants, indicating negligible modulation in spin susceptibility or density of states along that particular direction. A key contrast between the Cs and Rb variant is that the component out of the plane (K_{yy}) along the crystal c axis, the low T spectra of RbV_3Sb_5 exhibit two components without further resolvable splitting, consistent with a uniform TrH $2 \times 2 \times 2$ stacking structure [14,22,32]. However, in CsV_3Sb_5, by contrast, the single ^{51}V central line at 96 K develops a weak two-component structure at 95 K and, for $T < T_{CDW}$, further resolves into four components as each vanadium site splits into a Knight shift doublet (V1:V1′ and V2:V2′), as illustrated in Fig. 2(a). The field-linear dependence of the central transition splitting identifies a Knight shift origin rather than second-order quadrupolar effects. The additional modulation along the c axis, often described as a competition among $2 \times 2 \times 2$ and $2 \times 2 \times 4$ stackings with mixed layers of TrH and SoD, has been reported in diffraction and STM studies of CsV_3Sb_5 and is absent (within current resolution) in RbV_3Sb_5 and KV_3Sb_5 [9,10,14,33–36]. The temperature evolution of Knight shift anisotropy across T_{CDW} is consistent with a bond-centered, $3q$ CDW that reconstructs the Fermi surface and opens anisotropic, partially gapped spectra [4,36,37], with interlayer phase correlations mediated in part by Sb-derived states [38–40].

The temperature evolution of the integrated echo intensity corrected for Boltzmann polarization, $I(T)T$, provides a quantitative proxy for the number of nuclei contributing to the echo at fixed echo spacing. For the V1/V1′ and V2/V2′ families the quantities $I_{V_1}(T)T + I_{V_1'}(T)T$ and $I_{V_2}(T)T + I_{V_2'}(T)T$ decrease together upon cooling from 90 K to 75 K and then become temperature independent between 75 and 68 K; the total $I_{V_1}(T)T + I_{V_1'}(T)T + I_{V_2}(T)T + I_{V_2'}(T)T$ follows the same trend [Figs. 2(c) and 2(d)].

Between 90 and 75 K, the product $I(T)T$ extracted from two-pulse echoes at fixed echo spacing 2τ decreases even though the repetition time is long compared to T_1 and the central transition T_2 exhibits only modest fluctuations within experimental uncertainty, with no systematic decrease. For a half-integer quadrupolar nucleus such as ^{51}V (I=7/2), the central-transition Hahn-echo amplitude contains oscillatory envelope terms arising from second-order quadrupolar effects; the positions of nodes and antinodes shift with the EFG parameters ν_Q and η and with field orientation [41,42] As ν_Q and η evolve across the CDW regime of CsV_3Sb_5 [17,19], a fixed 2τ can move closer to an envelope minimum on cooling, thereby suppressing the echo amplitude although the long-time decay that defines T_2 remains essentially unchanged. In our data this short-time oscillatory envelope develops between 90 and 75 K as the CDW forms and then persists with approximately constant amplitude at lower temperatures; the effect is particularly evident for $2\tau \simeq 100$–110 μs (Fig. S6). A strong dependence of apparent spectral weight on the measurement timescale 2τ near charge order has been reported in other materials as well [43]. In addition, central-transition excitation is sensitive to flip angles and RF bandwidth: as $|\nu_Q|$ grows or the line shape widens, rectangular pulses underexcite portions of the central-transition manifold unless flip angles were reoptimized or broadband/frequency-stepped schemes were used [44,45]. For these reasons we do not interpret absolute $I(T)T$ as a volumetric measure in this temperature window. Instead, to quantify the interlayer modulation we analyze spectral-area ratios at fixed T of the doubled components,

$$R_i(T) = \frac{I_{V_i'}(T)}{I_{V_i}(T) + I_{V_i'}(T)} \qquad (i = 1, 2), \tag{1}$$

which are insensitive to global gain and to short-time envelope nodes at fixed T under identical acquisition conditions. The monotonic evolution of $R_1(T)$ and $R_2(T)$ evidences a redistribution among the layer-selective V environments that arise only in a $2 \times 2 \times 4$ interlayer modulation, consistent with synchrotron x-ray reports of temperature-driven reorganization/coexistence of $2 \times 2 \times 2$ and $2 \times 2 \times 4$ stackings in CsV_3Sb_5.

B. Quadrupolar EFG anomalies and first-order charge order at ~65 K

To interrogate charge-lattice modulations in CsV_3Sb_5 in the CDW state, we track the temperature evolution of the ^{51}V

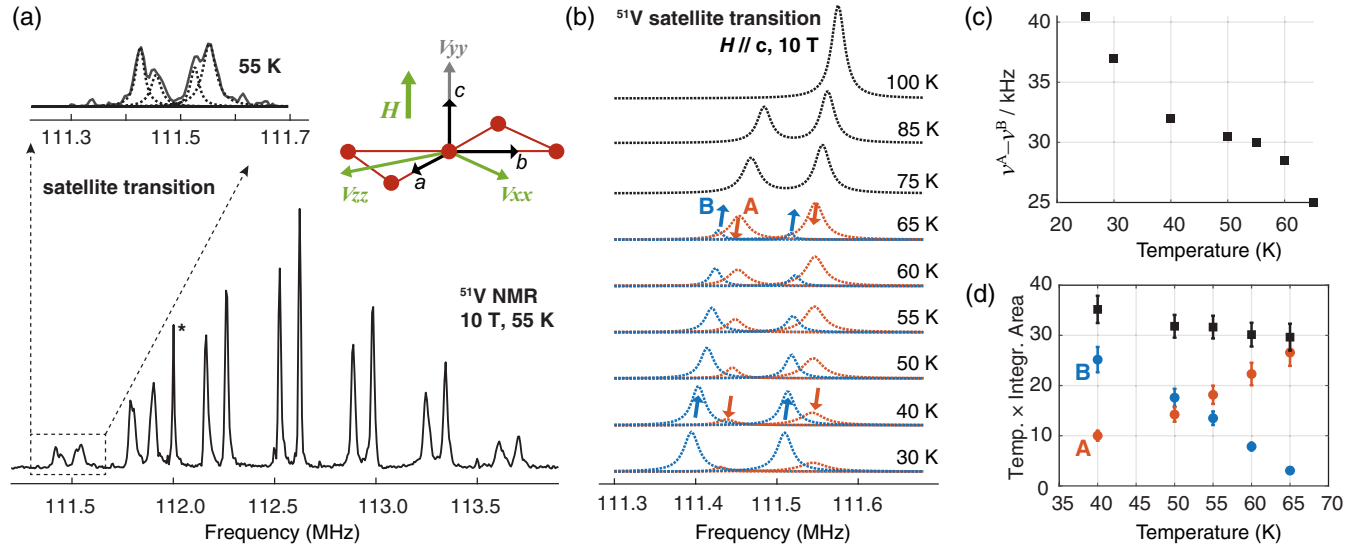

FIG. 3. ^{51}V quadrupolar satellites in CsV_3Sb_5 at the intermediate transition $T_{CO} \approx 65$ K ($H_0 \parallel c$) within the $2 \times 2 \times 4$ CDW background. (a) Representative spectrum at 55 K and 10 T; the expanded view highlights fitted satellite peaks for distinct in-plane EFG environments. (b) Temperature series of the fitted satellite transition manifolds showing the emergence of two well-resolved sets on cooling; spectra and fit overlays at the same temperatures are provided in Fig. S5. (c) Temperature dependence of the intermanifold splitting. (d) Relative spectral weights of the two EFG manifolds; the sum of integrated satellite intensity is conserved within experimental uncertainty. Error bars denote fit uncertainties. In (a), the asterisk (*) indicates the background ^{63}Cu NMR signal.

quadrupolar satellites with $H_0 \parallel c$ [Fig. 3(a)]. In this geometry the satellite frequencies are set by the in-plane principal components of the EFG tensor and their orientations with respect to H_0. Figure 3 summarizes the temperature evolution of the ^{51}V quadrupolar satellites across the intermediate temperature scale at $T_{CO} \approx 65$ K. On cooling through T_{CO} the spectra undergo an abrupt rearrangement: a single set of satellites above T_{CO} gives way to two well-resolved sets with distinct quadrupole splittings ν_Q^A and ν_Q^B, while the total integrated satellite intensity remains conserved within experimental uncertainty. The sudden appearance of two inequivalent EFG environments, the absence of critical broadening, and the persistence of two-component spectra over a finite-temperature interval are taken as evidence for a first-order transition at T_{CO} accompanied by in-plane phase segregation. In this regime the relative spectral weights of the two satellite manifolds evolve with temperature, whereas each ν_Q is nearly T independent, consistent with coexisting domains with different local EFGs whose volume fractions gradually interchange on cooling. Because two distinct satellite sets appear for $H_0 \parallel c$, the data demonstrate two groups of V sites with different EFG tensors. This observation is consistent with a reduction of the average in-plane rotational symmetry within the charge-ordered state, although NMR alone cannot fix the in-plane wave vector nor exclude multidomain or stacking-registry scenarios.

This intermediate transition is distinct from the primary CDW transition at $T_{CDW} \approx 94$ K in CsV_3Sb_5, which is already known to be first order and a $3q$ ground state. By contrast, prior work on the lower onset ($T \sim 60$–70 K) reported lattice/electronic anomalies but did not establish the order of the transition: coherent-phonon spectroscopy detected the emergence of an additional mode near $T^* \approx 60$ K and argued that this feature "appears at $T^* \approx 60$ K, well below T_{CDW}" and may be related to uniaxial ($1q$) order, possibly as a crossover or order-disorder phenomenon [16]; polarization-resolved Raman scattering modeled the anomaly with coupled primary/secondary like order parameters with T^* introduced phenomenologically (~70–80 K) but did not identify a thermodynamic phase transition [46,47]; and SI-STM observed $4a_0$ stripe order below ~60 K while emphasizing that targeted bulk scattering would be needed to determine whether the stripe order forms a bulk phase [13]. Our ^{51}V NMR data provide bulk, site-resolved evidence for a first-order transition at T_{CO}, thereby resolving this ambiguity. We do not observe ^{51}V T_1 anomaly across T_{CO}, consistent with prior ^{51}V NMR measurements [18,48].

In the context of the SI-STM observations [13], we thus attribute the two EFG environments below T_{CO} to stripe like charge order that breaks the in-plane sixfold symmetry of the CDW background. For the quadrupolar nucleus ^{51}V (I=7/2), we parametrize the EFG by principal components (V_{xx}, V_{yy}, V_{zz}) with $|V_{zz}| \geqslant |V_{yy}| \geqslant |V_{xx}|$ and define $\eta \equiv (V_{xx} - V_{yy})/V_{zz}$. In our convention informed by the refined structures, V_{zz} and V_{xx} lie approximately in plane while $V_{yy} \parallel c$, so η quantifies the in-plane vs out-of-plane charge anisotropy at vanadium sites. To relate the NMR signatures to specific structural models, we computed V-site EFGs using the synchrotron-refined structures of CsV_3Sb_5 at 90 and 11 K [14]. The 90 K models, representative of the interlayer-modulated $3q$ background above T_{CO}, yields a comparatively narrow spread of V_{zz} and η across V sites [Figs. 4(d) and 4(e)], whereas for the 11 K structure the calculated EFGs segregate into several well-separated clusters with larger η contrast [Fig. 4(a)], mirroring the discrete environments resolved in Fig. 3. It is worth noting that DFT calculations use the synchrotron-refined average mixed-layer structure at 11 K, hence predicting multiple vanadium sites at

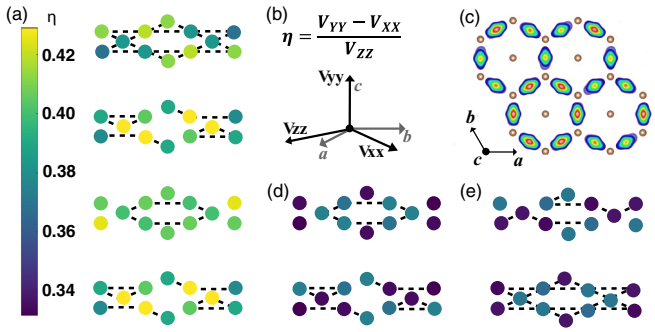

FIG. 4. DFT-calculated EFG anisotropy η and partial charge density for CsV_3Sb_5. Calculations use synchrotron-refined structures from Ref. [14] representative of (low-T) 11 K and (high-T) 90 K states. (a) Distribution of the EFG anisotropy η over V sites for the 11 K structure (color scale at left).(b) Orientation of principal EFG axes (V_{xx}, V_{yy}, V_{zz}) relative to crystal axes (a, b, c). (c) Partial charge density near E_F for the 11 K structure of CsV_3Sb_5. Real-space partial charge density associated with states within a narrow energy window around E_F (selected from the density of states peak; see Supplemental Material for the energy window and isovalue), computed for the synchrotron-refined 11 K structure and viewed along c (projected onto the kagome layer). (d),(e) Distributions of η for 90 K structures.

lower temperatures, whereas the weight transfer between EFG domains (A/B) reflects single-variant selection at temperatures below T_{CO}.

Within these structural models, the orbital-resolved partial charge densities near E_F [Fig. 4(c)] show a stronger, directional V-3d/Sb-5p mixing anisotropy at 11 K than at 90 K. This trend accords with temperature-dependent x-ray absorption and DFT that identify V3d-Sb5p hybridization as a key contributor to the CDW transition in CsV_3Sb_5 [49], and with resonant x-ray scattering that reveals an Sb-5p–assisted $2\times2\times2$ component conjoined with the kagome-plane $2\times2\times1$ order in the three-dimensional CDW state [50].

IV. CONCLUSION

Orientation-dependent ^{51}V NMR on CsV_3Sb_5, with RbV_3Sb_5 as a reference, yields two findings. First, CsV_3Sb_5 exhibits an interlayer-modulated $3q$ charge order whose local environments are consistent with a $2 \times 2 \times 4$ stacking, while RbV_3Sb_5 shows the uniform TrH $2 \times 2 \times 2$ order; this provides a bulk, site-selective discriminator between these three-dimensional CDW microstructures. Second, at $T_{CO} \approx 65$ K and for $H_0 \parallel c$, the ^{51}V spectra reveal two inequivalent EFG environments that appear and coexist over a finite interval, indicating a reduction of the average in-plane rotational symmetry within the charge-ordered state.

The two-manifold spectra further indicate in-plane phase segregation and, together with conserved total satellite intensity and nearly temperature-independent ν_Q within each manifold, establish the bulk first-order character at T_{CO}. NMR does not determine the in-plane wave vector and we therefore refrain from assigning a microscopic nematic mechanism; the data are, however, compatible with a uniaxial component reported by surface probes. DFT calculations based on synchrotron-refined 90 and 11 K structures capture the evolution from a narrow to a clustered distribution of EFG local tensors, consistent with inequivalent V environments. These results provide a quantitative, site-selective benchmark for distinguishing $2 \times 2 \times 4$ from $2 \times 2 \times 2$ stacking in the 135 kagome family.

ACKNOWLEDGMENTS

We thank Stuart Brown, Riku Yamamoto, Tri Thanh Chau (University of California, Los Angeles), and Rong Cong (National High Magnetic Field Laboratory) for insightful discussions. X.W. and B.R.O. were supported by the U.S. Department of Energy, Office of Science, Office of Basic Energy Sciences, under Award No. DE-SC0025712. NMR measurements were performed at the National High Magnetic Field Laboratory, which is supported by the National Science Foundation under Cooperative Agreement No. DMR-2128556 and the State of Florida. A.C.S., B.R.O., and S.D.W. gratefully acknowledge support via the UC Santa Barbara NSF Quantum Foundry funded via the Q-AMASE-i program under award DMR-1906325. H.B. acknowledges the generous computing resources provided by the Sulis HPC service (EP/T022108/1), ARCHER2 UK National Computing Service, which was granted via HPC-CONEXS, the UK High-End Computing Consortium (EPSRC Grant No. EP/X035514/1).

X.W. collected and analyzed the NMR data; A.P.R. provided experimental support for the NMR measurements; B.R.O., A.C.S., and S.D.W. provided samples; and H.B. performed the DFT calculations.

DATA AVAILABILITY

The data that support the findings of this article are not publicly available. The data are available from the authors upon reasonable request.

[1] Brenden R. Ortiz, Lidia C. Gomes, Jennifer R. Morey, M. Winiarski, M. Bordelon, John S. Mangum, Iain W. H. Oswald, J. A. Rodriguez-Rivera, James R. Neilson, Stephen D. Wilson, E. Ertekin, T. M. McQueen, and Eric S. Toberer, New kagome prototype materials: Discovery of KV_3Sb_5, RbV_3Sb_5, and CsV_3Sb_5, Phys. Rev. Mater. **3**, 094407 (2019).

[2] Brenden R. Ortiz, Samuel M. L. Teicher, Y. Hu, Julia L. Zuo, Paul M. Sarte, Emily C. Schueller, A. M. Milinda Abeykoon, Mathew J. Krogstad, S. Rosenkranz, R. Osborn, R. Seshadri, L. Balents, J. He, and Stephen D. Wilson, CsV_3Sb_5:A $\mathbb{Z}_2$ topological kagome metal with a superconducting ground state, Phys. Rev. Lett. **125**, 247002 (2020).

[3] Q. Yin, Z. Tu, C. Gong, Y. Fu, S. Yan, and H. Lei, Superconductivity and normal-state properties of kagome metal RbV_3Sb_5 single crystals, Chin. Phys. Lett. **38**, 037403 (2021).

[4] H. Tan, Y. Liu, Z. Wang, and B. Yan, Charge density waves and electronic properties of superconducting kagome metals, Phys. Rev. Lett. **127**, 046401 (2021).

[5] M. Kang, S. Fang, L. Ye, H. C. Po, J. Denlinger, C. Jozwiak, A. Bostwick, E. Rotenberg, E. Kaxiras, J. G. Checkelsky, and R. Comin, Twofold van hove singularity and origin of charge order in topological kagome superconductor CsV_3Sb_5, Nat. Phys. **18**, 301 (2022).

[6] Y. Hu, S. M. L. Teicher, B. R. Ortiz, Y. Luo, S. Peng, L. Huai, J. Ma, N. C. Plumb, S. D. Wilson, J. He, and M. Shi, Rich nature of van hove singularities in kagome superconductor CsV_3Sb_5, Nat. Commun. **13**, 2220 (2022).

[7] Morten H. Christensen, T. Birol, Brian M. Andersen, and Rafael M. Fernandes, Theory of the charge density wave in AV_3Sb_5 kagome metals, Phys. Rev. B **104**, 214513 (2021).

[8] H. LaBollita and Antia S. Botana, Tuning the van Hove singularities in AV_3Sb_5(A = K, Rb, Cs) via pressure and doping, Phys. Rev. B **104**, 205129 (2021).

[9] H. Li, T. T. Zhang, T. Yilmaz, Y. Y. Pai, C. E. Marvinney, A. Said, Q. W. Yin, C. S. Gong, Z. J. Tu, E. Vescovo, C. S. Nelson, R. G. Moore, S. Murakami, H. C. Lei, H. N. Lee, B. J. Lawrie, and H. Miao, Observation of unconventional charge density wave without acoustic-phonon anomaly in kagome superconductors AV_3Sb_5(A = Rb, Cs), Phys. Rev. X **11**, 031050 (2021).

[10] Z. Liang, X. Hou, F. Zhang, W. Ma, P. Wu, Z. Zhang, F. Yu, J. J. Ying, K. Jiang, L. Shan, Z. Wang, and X.-H. Chen, Three-dimensional charge density wave and surface-dependent vortex-core states in a kagome superconductor CsV_3Sb_5, Phys. Rev. X **11**, 031026 (2021).

[11] Brenden R. Ortiz, Samuel M. L. Teicher, L. Kautzsch, Paul M. Sarte, N. Ratcliff, J. Harter, Jacob P. C. Ruff, R. Seshadri, and Stephen D. Wilson, Fermi surface mapping and the nature of charge-density-wave order in the kagome superconductor CsV_3Sb_5, Phys. Rev. X **11**, 041030 (2021).

[12] M. Kang, S. Fang, L. Ye, J. S. You, S. Fang, A. Levitan, M. Han, C. Jozwiak, A. Bostwick, E. Rotenberg, E. Kaxiras, J. G. Checkelsky, and R. Comin, Charge order landscape and competition with superconductivity in kagome metals, Nat. Mater. **22**, 186 (2023).

[13] H. Zhao, H. Li, B. R. Ortiz, S. D. Wilson, and M. Z. Hasan, Cascade of correlated electron states in a kagome superconductor CsV_3Sb_5, Nature (London) **599**, 216 (2021).

[14] L. Kautzsch, Brenden R. Ortiz, K. Mallayya, J. Plumb, G. Pokharel, Jacob P. C. Ruff, Z. Islam, Eun A. Kim, R. Seshadri, and Stephen D. Wilson, Structural evolution of the kagome superconductors AV_3Sb_5 (A = K, Rb, and Cs) through charge-density-wave order, Phys. Rev. Mater. **7**, 024806 (2023).

[15] G. Liu, X. Ma, K. He, Q. Li, H. Tan, Y. Liu, J. Xu, W. Tang, K. Watanabe, T. Taniguchi, L. Gao, Y. Dai, H.-H. Wen, B. Yan, and X. Xi, Observation of anomalous amplitude modes in the kagome metal CsV_3Sb_5, Nat. Commun. **13**, 3461 (2022).

[16] N. Ratcliff, L. Hallett, Brenden R. Ortiz, Stephen D. Wilson, and John W. Harter, Coherent phonon spectroscopy and interlayer modulation of charge density wave order in the kagome metal CsV_3Sb_5, Phys. Rev. Mater. **5**, L111801 (2021).

[17] C. Mu, Q. Yin, Z. Tu, C. Gong, H. Lei, Z. Li, and J. Luo, S-wave superconductivity in kagome metal CsV_3Sb_5 revealed by $^{121/123}$Sb NQR and ^{51}V NMR measurements, Chin. Phys. Lett. **38**, 077402 (2021).

[18] D.-W. Song, L.-X. Zheng, F.-H. Yu, J. Li, L.-P. Nie, M. Shan, D. Zhao, S.-J. Li, B.-L. Kang, Z.-M. Wu, Y.-B. Zhou, K.-L. Sun, K. Liu, X.-G. Luo, Z.-Y. Wang, J.-J. Ying, X.-G. Wan, T. Wu, and X.-H. Chen, Orbital ordering and fluctuations in a kagome superconductor CsV_3Sb_5, Sci. China: Phys. Mech. Astron. **65**, 247462 (2022).

[19] J. Luo, N. W. Wang, D. X. Zhang, L. M. Zhang, Z. Y. Wang, H. Y. Ma, R. Zhang, S. J. Tian, Y. F. Zhang, H. C. Lei, J. Q. Yan, D. G. Mandrus, and Y. H. Zhang, Possible star-of-david pattern charge density wave with additional modulation in the kagome superconductor CsV_3Sb_5, npj Quantum Mater. **7**, 30 (2022).

[20] L. Zheng, Z. Wu, Y. Yang, L. Nie, M. Shan, K. Sun, D. Song, F. Yu, J. Li, D. Zhao, S. Li, B. Kang, Y. Zhou, K. Liu, Z. Xiang, J. Ying, Z. Wang, T. Wu, and X. Chen, Emergent charge order in pressurized kagome superconductor CsV_3Sb_5, Nature (London) **611**, 682 (2022).

[21] X. Y. Feng, Z. Zhao, J. Luo, J. Yang, A. F. Fang, H. T. Yang, H. J. Gao, R. Zhou, and G.-q. Zheng, Commensurate-to-incommensurate transition of charge-density-wave order and a possible quantum critical point in pressurized kagome metal CsV_3Sb_5, npj Quantum Mater. **8**, 23 (2023).

[22] J. Frassineti, P. Bonfà, G. Allodi, E. Garcia, R. Cong, Brenden R. Ortiz, Stephen D. Wilson, R. De Renzi, Vesna F. Mitrović, and S. Sanna, Microscopic nature of the charge-density wave in the kagome superconductor RbV_3Sb_5, Phys. Rev. Res. **5**, L012017 (2023).

[23] X. Zhang, Y. Li, J. Zheng, F. Zhou, Q. Wu, X. Xi, Y. Lau, Z. Wang, and W. Wang, NMR study of charge density wave phase in the kagome metal RbV_3Sb_5, Appl. Phys. Lett. **124**, 093106 (2024).

[24] X. Y. Feng, Z. Zhao, J. Luo, Y. Z. Zhou, J. Yang, A. F. Fang, H.-T. Yang, H.-J. Gao, R. Zhou, and G.-q. Zheng, Fully-gapped superconductivity with rotational symmetry breaking in pressurized kagome metal CsV_3Sb_5, Nat. Commun. **16**, 3643 (2025).

[25] Yuzki M. Oey, Brenden R. Ortiz, F. Kaboudvand, J. Frassineti, E. Garcia, R. Cong, S. Sanna, Vesna F. Mitrović, R. Seshadri, and Stephen D. Wilson, Fermi level tuning and double-dome superconductivity in the kagome metal $CsV_3Sb_{5-x}Sn_x$, Phys. Rev. Mater. **6**, L041801 (2022).

[26] A. N. Capa Salinas, B. R. Ortiz, C. Bales, J. Frassineti, V. F. Mitrović, and S. D. Wilson, Electron–hole asymmetry in the phase diagram of carrier-tuned CsV_3Sb_5, Front. Electron. Mater. **3**, 1257490 (2023).

[27] See Supplemental Material at http://link.aps.org/supplemental/10.1103/91c9-z267 for experimental details of ^{51}V NMR and DFT calculations with additional band-structure data.

[28] P. E. Blöchl, Projector augmented-wave method, Phys. Rev. B **50**, 17953 (1994).

[29] G. Kresse and J. Hafner, *Ab initio* molecular dynamics for liquid metals, Phys. Rev. B **47**, 558 (1993).

[30] G. Kresse and J. Furthmüller, Efficient iterative schemes for *ab initio* total-energy calculations using a plane-wave basis set, Phys. Rev. B **54**, 11169 (1996).

[31] John P. Perdew, K. Burke, and M. Ernzerhof, Generalized gradient approximation made simple, Phys. Rev. Lett. **77**, 3865 (1996).

[32] M. Wenzel, B. R. Ortiz, S. D. Wilson, M. Dressel, A. A. Tsirlin, and E. Uykur, Optical study of RbV_3Sb_5: Multiple

density-wave gaps and phonon anomalies, Phys. Rev. B **105**, 245123 (2022).

[33] Q. Stahl, D. Chen, T. Ritschel, C. Shekhar, E. Sadrollahi, M. C. Rahn, O. Ivashko, M. v. Zimmermann, C. Felser, and J. Geck, Temperature-driven reorganization of electronic order in CsV_3Sb_5, Phys. Rev. B **105**, 195136 (2022).

[34] Q. Xiao, Y. Lin, Q. Li, X. Zheng, S. Francoual, C. Plueckthun, W. Xia, Q. Qiu, S. Zhang, Y. Guo, J. Feng, and Y. Peng, Coexistence of multiple stacking charge density waves in kagome superconductor CsV_3Sb_5, Phys. Rev. Res. **5**, L012032 (2023).

[35] Y.-X. Jiang, J.-X. Yin, M. M. Denner, N. Shumiya, B. R. Ortiz, G. Xu, Z. Guguchia, J. He, M. S. Hossain, X. Liu *et al.*, Unconventional chiral charge order in kagome superconductor KV_3Sb_5, Nat. Mater. **20**, 1353 (2021).

[36] T. Kato, Y. Li, T. Kawakami, M. Liu, K. Nakayama, Z. Wang, A. Moriya, K. Tanaka, T. Takahashi, Y. Yao, and T. Sato, Three-dimensional energy gap and origin of charge-density wave in kagome superconductor KV_3Sb_5, Commun. Mater. **3**, 30 (2022).

[37] K. Nakayama, Y. Li, T. Kato, M. Liu, Z. Wang, T. Takahashi, Y. Yao, and T. Sato, Multiple energy scales and anisotropic energy gap in the charge-density-wave phase of the kagome superconductor CsV_3Sb_5, Phys. Rev. B **104**, L161112 (2021).

[38] M. Y. Jeong, Hyeok-J. Yang, H. S. Kim, Y. B. Kim, S. B. Lee, and M. J. Han, Crucial role of out-of-plane sb p orbitals in van hove singularity formation and electronic correlations in the superconducting kagome metal CsV_3Sb_5, Phys. Rev. B **105**, 235145 (2022).

[39] Ethan T. Ritz, Rafael M. Fernandes, and T. Birol, Impact of sb degrees of freedom on the charge density wave phase diagram of the kagome metal CsV_3Sb_5, Phys. Rev. B **107**, 205131 (2023).

[40] H. Li, X. Liu, Y. B. Kim, and Hae-Y. Kee, Origin of π-shifted three-dimensional charge density waves in the kagome metal AV_3Sb_5 (A = K, Rb, and Cs), Phys. Rev. B **108**, 075102 (2023).

[41] P. P. Man, Second-order quadrupole effects on Hahn echoes in fast-rotating solids at the magic angle, Phys. Rev. B **55**, 8406 (1997).

[42] R. D. Walker and B. C. Gerstein, Second-order quadrupolar echo, Phys. Rev. B **31**, 3167 (1985).

[43] T. Imai, S. K. Takahashi, A. Arsenault, A. W. Acton, D. Lee, W. He, Y. S. Lee, and M. Fujita, Revisiting ^{63}Cu NMR evidence for charge order in superconducting $La_{1.885}Sr_{0.115}CuO_4$, Phys. Rev. B **96**, 224508 (2017).

[44] L. A. O'Dell, K. J. Harris, and R. W. Schurko, Optimized excitation pulses for the acquisition of static NMR powder patterns from half-integer quadrupolar nuclei, J. Magn. Reson. **203**, 156 (2010).

[45] H.-T. Kwak, J. Tang, P. R. Vasconcelos, D. K. Lee, D. P. Weitekamp, C. J. Pike, D. P. Weliky, G. S. Boutis, and T. M. J. Grandinetti, Selective suppression and excitation of solid-state NMR resonances based on quadrupole coupling constants, J. Magn. Reson. **160**, 107 (2003).

[46] S. Wu, Brenden R. Ortiz, H. Tan, Stephen D. Wilson, B. Yan, T. Birol, and G. Blumberg, Charge density wave order in the kagome metal AV_3Sb_5 (A = Cs, Rb, K), Phys. Rev. B **105**, 155106 (2022).

[47] D. Wulferding, S. Lee, Y. Choi, Q. Yin, Z. Tu, C. Gong, H. Lei, S. Yousuf, J. Song, H. Lee, T. Park, and Kwang-Y. Choi, Emergent nematicity and intrinsic versus Extrinsic electronic scattering processes in the kagome metal CsV_3Sb_5, Phys. Rev. Res. **4**, 023215 (2022).

[48] L. Nie*et al.*, Charge-density-wave-driven electronic nematicity in a kagome superconductor, Nature (London) **604**, 59 (2022).

[49] S. Han, C. S. Tang, L. Li, Y. Liu, H. Liu, J. Gou, J. Wu, D. Zhou, P. Yang, C. Diao*et al.*, Orbital-hybridization-driven charge density wave transition in CsV_3Sb_5 kagome superconductor, Adv. Mater. **35**, 2209010 (2023).

[50] H. Li, G. Fabbris, A. H. Said, Y. Pai, Q. Yin, C. Gong, Z. Tu, H. Lei, P. Sun, S. D. Wilson, B. Yan, R. Thomale, and H. Miao, Discovery of Conjoined charge density waves in the kagome superconductor CsV_3Sb_5, Nat. Commun. **13**, 6348 (2022).